Metal Oxide Nanoparticles for Asphaltene Adsorption and Oxidation

ARTICLE *in* ENERGY & FUELS · JANUARY 2011

Impact Factor: 2.79 · DOI: 10.1021/ef101230g

3 AUTHORS, INCLUDING:

Nashaat N Nassar
The University of Calgary
65 PUBLICATIONS **887** CITATIONS
SEE PROFILE

Azfar Hassan
The University of Calgary
36 PUBLICATIONS **386** CITATIONS
SEE PROFILE

energy&fuels

ARTICLE

pubs.acs.org/EF

Metal Oxide Nanoparticles for Asphaltene Adsorption and Oxidation

Nashaat N. Nassar,[†,‡] Azfar Hassan,[†,‡] and Pedro Pereira-Almao*[,†,‡]

[†]Alberta Ingenuity Centre for In-Situ Energy, University of Calgary, Calgary, Alberta, Canada

[‡]Department of Chemical & Petroleum Engineering, University of Calgary, Calgary, Alberta, Canada

ABSTRACT: This study investigates the adsorption and oxidation of asphaltenes onto nanoparticles. Six different metal oxide nanoparticles were employed, namely, Fe_3O_4, Co_3O_4, TiO_2, MgO, CaO, and NiO. Batch adsorption experiments were carried out at different initial asphaltene concentrations. Asphaltene adsorption was evaluated by measuring the asphaltene concentration using thermogravimetric analysis, and adsorption kinetics and isotherms were obtained. For all the six nanoparticles, the isotherm data fitted well to the Langmuir model. Results showed that asphaltene adsorption is metal-oxide-specific and the adsorption capacities of asphaltenes onto the oxides followed the order CaO > Co_3O_4 > Fe_3O_4 > MgO > NiO > TiO_2. Furthermore, oxidation of asphaltene was investigated after adsorption onto NiO nanoparticles. The oxidation temperature of asphaltene decreased by ~140 °C in the presence of nanoparticles, showing their catalytic effect. The activation energies calculated by the Coats−Redfern method for asphaltene oxidation processes in the absence and presence of NiO nanoparticles were found to be approximately 100 and 57 kJ/mol, respectively. This study is a first step in showing the feasibility of using nanoparticles for asphaltene adsorption, followed by catalytic oxidation for heavy oil upgrading.

1. INTRODUCTION

Currently, the oil sands recovery and upgrading processes are more water and energy intensive; as a result, more pollution is created, such as heavier residue, wastewater, solid waste, and air emissions.[1−4] This has resulted in opportunities for development of new technologies that improve heavy oil recovery, minimize the use of energy and water-based processes, and reduce the air emissions with lower-cost services.

Nanotechnology is making a significant impact on various industrial applications.[5−9] Nanoparticles are one of the important examples on nanotechnology applications. Because of their unique properties, nanoparticles can be used to sustain the oil sands industry through the development of greener processes with a cost-effective approach. Asphaltenes are aromatic macromolecules containing heteroatoms present in a heavy oil matrix, which makes heavy oil difficult to upgrade and process.[10−14] Removal of asphaltenes from crude oil has, therefore, great significance. This study looks at heavy oil upgrading by the removal of asphaltenes with nanoparticles, followed by oxidation. By integrating asphaltene adsorption and oxidation, important synergies would be realized. These include reduction in capital cost, increase in energy efficiency, and enhanced performance and portability.[15] In this work, six different commercially available metal oxide nanoparticles, namely, Fe_3O_4, Co_3O_4, TiO_2, MgO, CaO, and NiO, were selected for asphaltene adsorption and oxidation. These metal oxides can be divided into acidic, basic, and amphoteric metal oxides, thus covering the broad spectrum. Adsorption and oxidation of asphaltenes were studied using thermogravimetric analysis. Thermogravimetric analysis (TGA) has been useful in crude oil characterization and combustion studies.[16−19] Useful data, such as reaction rates, heat of reaction, and activation energy, can be collected in a short time. Researchers using TGA have identified various oxidation regions and calculated activation energies for the oxidation processes.[18]

To the best of our knowledge, a study on adsorption of asphaltenes onto nanoparticles followed by catalytic oxidation of adsorbed asphaltenes is conducted for the first time.

2. EXPERIMENTAL SECTION

2.1. Materials. Six commercially available metal oxide nanoparticles (Fe_3O_4, Co_3O_4, TiO_2, MgO, CaO, and NiO) were used in this study. Fe_3O_4 was obtained from Nanostructured & Amorphous Materials, Inc., TX, USA. The rest were obtained from Sigma Aldrich, ON. Model solutions of precipitated asphaltenes redissolved in toluene were prepared. Asphaltenes were extracted from Athabasca vacuum residue. Solvents used in the precipitation and extraction were *n*-heptane (99% HPLC grade, Sigma Aldrich, ON), *n*-pentane (99% HPLC grade, Sigma Aldrich, ON), and toluene (analytical grade, EMD, Merck, NJ).

2.2. Methods. *2.2.1. Estimation of Specific Surface Areas of Selected Nanoparticles.* The surface area was measured by performing N_2 adsorption and desorption at 77 K, using a Micromeretics Tristar 2000 surface area analyzer. The samples were degassed at 150 °C under a N_2 flow overnight before analysis. Surface areas were calculated using the Brunauer−Emmet−Teller (BET) equation. External surface areas were obtained by the *t*-plot method, and there was no significant difference between the surface areas obtained by the BET and *t*-plot methods. This indicates that these nanoparticles are essentially nonporous. It is worth mentioning that the nanoparticle powders were present as aggregates, which made their surface area measurement possible.

2.2.2. Preparation of Heavy Oil Model Solutions. Asphaltenes were extracted from Athabasca vacuum residue with addition of *n*-heptane as follows, unless otherwise noted. A specified amount of vacuum residue was liquefied by heating to ~100 °C and mixed with *n*-heptane at a 1:40 (g/mL) ratio. The solution was then sonicated in a water bath at 25 °C for 2 h and left shaking at 300 rpm for 1 day to equilibrate. Black

Received: September 11, 2010
Revised: January 4, 2011
Published: January 21, 2011

precipitated asphaltenes settled at the bottom and then were collected after decanting the supernatant. The precipitated asphaltenes were then washed with fresh *n*-heptane at a ratio of 1:4 (g/mL) and centrifuged at 5000 rpm for 5 min and left to stand overnight. The asphaltenes were separated from the final solution by filtration using an 8 μm Whatman filter paper. The cake was washed with *n*-heptane several times until the color of the asphaltenes became shiny black. The resultant asphaltenes were homogenized and fined using a pestle and mortar and left to dry at room temperature in a hood until no change in mass was observed. The resultant recovery yield was 15 wt %, which is in the range reported in the literature.[20,21] The resultant asphaltene was labeled as C7-asphaltenes. A similar procedure was used to prepare C5-aspahltenes; in this case, *n*-pentane was used as a precipitant instead of *n*-heptane and the recovery yield was around 20 wt %.

The model solutions for the batch adsorption experiments were prepared by dissolving a certain amount of the asphaltenes in toluene. All samples were prepared from a stock solution containing 5000 ppm asphaltenes diluted to different concentrations by addition of toluene. The initial concentration of asphaltene solutions used in the adsorption experiments ranged from 150 to 3000 ppm.

2.2.3. Adsorption Experiments. Adsorption of asphaltenes onto the nanoparticles was performed at 25 °C. Batch adsorption experiments were carried out by adding a certain mass of the nanoparticles to 10 mL of an asphaltenes−toluene solution at a ratio of nanoparticles to model heavy oil solution of 10:1 (g/L). The vials were tightly sealed to avoid loss of toluene by evaporation and shaken at 200 rpm in an incubator at 25 °C until equilibrium was established. The nanoparticle-containing asphaltenes were then separated via centrifugation at 5000 rpm for 30 min. The supernatant was decanted, and the precipitate (i.e., nanoparticles containing adsorbed asphaltenes) was placed in a vacuum oven at 60 °C for 24 h to evaporate any remaining toluene. After drying, the sample was subjected to thermal analysis.

2.2.4. Thermogravimetric Analysis of Asphaltenes. The amount of adsorbed asphaltenes onto nanoparticles was obtained from the mass loss determined by a thermogravimetric analyzer, TGA (Q600, TA Instruments, Inc., NJ) between 200 and 600 °C. Thermogravimetric analysis of asphaltenes, nanoparticles, and nanoparticles containing adsorbed asphaltenes was carried out using TGA. About 5 mg of the samples was heated under an air atmosphere. The sample mass was kept low to avoid diffusion limitations. The flow rate of air was kept at 100 cm^3/min. Fresh nanoparticles from the original bottle were heated to 1000 °C at a heating rate of 10 °C/min to get a complete profile of mass loss and heat changes. For adsorption kinetics and isotherms, pure asphaltenes and asphaltenes adsorbed onto nanoparticles were heated to 900 °C in air at a heating rate of 10 °C/min. The amount of adsorbed asphaltenes was calculated as follows: (1) Known mass of fresh nanoparticles were analyzed by the TGA, and the residual mass was recorded; (2) nanoparticles containing adsorbed asphaltenes were also analyzed by the TGA, and the residual mass and the mass loss were recorded; and (3) the mass of adsorbed asphaltenes was estimated from steps 1 and 2. Subsequently, the equilibrium concentration of asphaltenes in the supernatant, C_e, and the amount adsorbed (Q_e, mass of adsorbed asphaltenes/mass of nanoparticles) are calculated from the mass balance as the initial concentration of asphaltenes and the mass of nanoparticles are known. For activation energy studies, the mass loss and heat changes up to 600 °C were recorded in separate experiments and used in calculations. Each run was repeated twice, to confirm the reproducibility of the experiment.

3. RESULTS AND DISCUSSION

3.1. Textural Properties of Nanoparticles. Table 1 lists the specifications and textural properties of nanoparticles used in our study. As seen in Table 1, there is no significant difference between BET and *t*-plot surface area values, which indicates that the nanoparticles considered in this study are essentially nonporous.

Table 1. Surface Properties and Chemical Nature of Selected Metal Oxide Nanoparticles

nanoparticles	particle diameter[a] (nm)	specific surface area (BET) (m^2/g)	external S.A. (m^2/g)	chemical nature
Co_3O_4	<50	41	39	amphoteric
Fe_3O_4	20−30	43	37	amphoteric
MgO	<50	82	79	basic
CaO	<160	31	29	basic
TiO_2	<25	183	194	acidic
NiO	<50	107	94	acidic

[a] Manufacturer reported.

TiO_2 and NiO nanoparticles showed high surface areas as compared with other nanoparticles considered in this study.

3.2. Adsorption Isotherms. Adsorption isotherms were conducted for the selected nanoparticles at 25 °C by varying the initial concentration of asphaltenes from 150 to 3000 ppm. Figure 1 shows the adsorption isotherms of asphaltenes onto nanoparticles. The shape of the isotherms was fitted to Freundlich and Langmuir models,[22,23] which are expressed in eqs 1 and 2, respectively.

$$Q_e = K_F C_e^{1/n} \quad (1)$$

$$Q_e = Q_m \frac{K_L C_e}{1 + K_L C_e} \quad (2)$$

The linear forms of the Freundlich and Langmuir models are given by eqs 3 and 4, respectively

$$\log(Q_e) = \log(K_F) + \frac{1}{n}\log(C_e) \quad (3)$$

$$\frac{C_e}{Q_e} = \frac{1}{Q_m K_L} + \frac{C_e}{Q_m} \quad (4)$$

where Q_e is the amount of asphaltenes adsorbed onto the nanoparticles (mg/m^2), C_e is the equilibrium concentration of asphaltenes in solution phase (mg/L), and K_F and $1/n$ are Freundlich constants. K_F is roughly an indicator of the adsorption capacity ((mg/m^2)(L/mg)$^{1/n}$), and $1/n$ is the adsorption intensity factor (unitless). Accordingly, a larger K_F value suggests a greater adsorption capacity, and a lower $1/n$ value indicates stronger adsorption strength. K_L is the Langmuir equilibrium adsorption constant related to the affinity of binding sites (L/mg), and Q_m is the maximum amount of adsorbed asphaltenes per unit surface area of nanoparticles for complete monolayer coverage (mg/m^2). Langmuir-type isotherms were reported for adsorption of asphaltenes onto clay[11,24,25] and minerals,[26] whereas Marczewski and Szymula[27] reported an increasing trend of asphaltene adsorption onto minerals, characterized by two steps, which indicated changes in the colloidal state of asphaltenes. Those changes were considered to be due to asphaltene self-association and further formation of hemimicelles and micelles.[27] It is noteworthy to mention that the Langmuir model assumed that adsorptions occur on a homogeneous surface with monolayer coverage, whereas the Freundlich model describes adsorption where the adsorbent has a heterogeneous surface with adsorption sites that have different adsorption energies. As seen in Figure 1, for all selected nanoparticles, asphaltene adsorption increased sharply at low equilibrium concentration

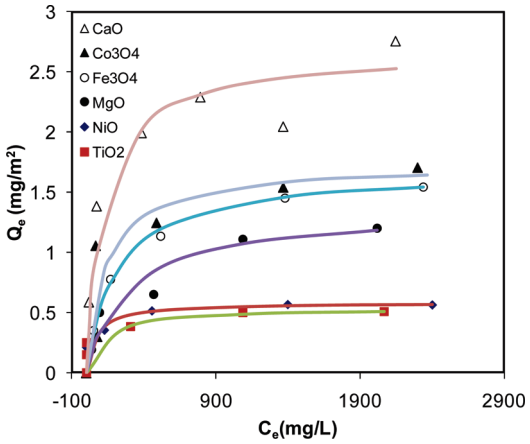

Figure 1. Adsorption isotherm of asphaltenes onto different nanoparticles. Nanoparticle dose, 10 g/L; agitation speed, 200 rpm; *T*, 25 °C. The symbols are experimental data, and the solid lines are from the Langmuir model (eq 2).

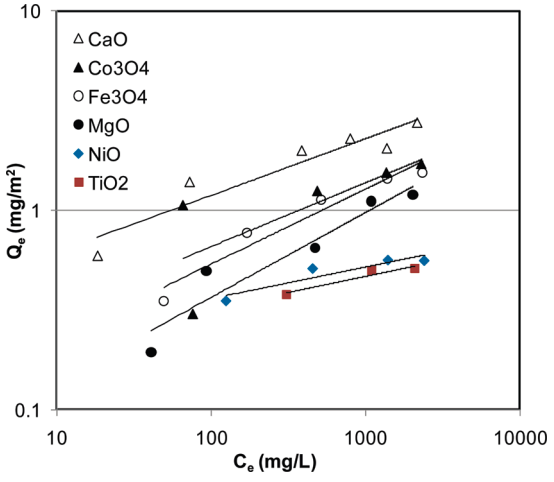

Figure 2. Freundlich adsorption isotherm of asphaltenes onto different nanoparticles. Nanoparticle dose, 10 g/L; agitation speed, 200 rpm; *T*, 25 °C. The symbols are experimental data, and the solid lines are from the linearized Freundlich model (eq 3).

and starts to level off with further increases of asphaltene concentration. The Freundlich and Langmuir linear plots are presented in Figures 2 and 3, respectively. Clearly, the Langmuir model seems to be the best-fitting model for the experimental data. The adsorption equilibrium data for all selected nanoparticles fitted very well to the Langmuir model with correlation coefficients in the range from 0.96 to 1.0. Langmuir and Freundlich fitted parameters are tabulated in Table 2. It can be observed that the Q_m value differs widely for different nanoparticles. A comparison of Q_m values shows that the CaO exhibits the highest adsorption capacity. It appears that basic and amphoteric oxides have high adsorption capacity as compared with acidic oxides, for example, NiO and TiO_2.

3.3. Affinity of Asphaltenes toward Metal Oxide Surfaces.

The adsorption of asphaltenes onto surfaces depends on the type and strength of interactions between the asphaltenes and the surface. Therefore, Langmuir parameters were further investigated to examine the level of involvement of various surfaces of the metal oxides in bonding to the asphaltenes.

All the oxides considered in this study showed high adsorption capacity, Q_m, and affinity, K_L. Interestingly, Q_m and K_L values are

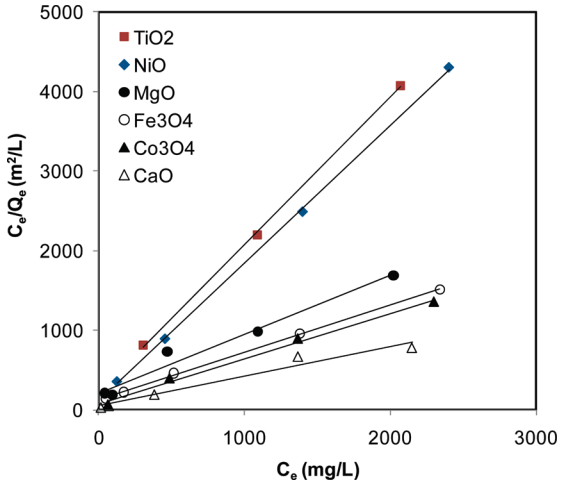

Figure 3. Langmuir adsorption isotherm of asphaltenes onto different nanoparticles. Nanoparticle dose, 10 g/L; agitation speed, 200 rpm; *T*, 25 °C. The symbols are experimental data, and the solid lines are from the linearized Langmuir model (eq 4).

metal-oxide-specific, and the ranking of Q_m and K_L is completely different. For instance, the Q_m of the selected oxides followed the order CaO > Co_3O_4 > Fe_3O_4 > MgO > NiO > TiO_2, whereas K_L has the following order NiO > TiO_2 > CaO > Co_3O_4 > Fe_3O_4 > MgO. These differences can be attributed to a different degree of interaction between metal oxide surface and asphaltenes. Similar observations were reported by other researchers for adsorption of asphaltenes onto different minerals and clays.[28] Most of the previous investigators used oxygen-containing adsorbents.[24−26,29−32] In those studies, the various hypotheses attributed asphaltene adsorption to bonding between asphaltenes and the surface resulting from functionalized groups on the asphaltenes, including carboxylic, pyrrolic, pyridininc, thiophenic, and sulphite.[33] González et al.[32] reported that the presence of oxygen and nitrogen in the structure of asphaltenes plays an important role in the adsorption rate and capacity. Fritschy and Papirer-Fillers[34] concluded that asphaltenes undergo chemisorption on the silanol groups of the silica. Others highlighted the involvement of surface charge at the interface in bonding asphaltenes to the surface.[14,25,35] On the other hand, Drummond and Israelachvili[36] suggested that van der Waals forces between the surface and the asphaltenes in the oil is the binding force of the asphaltene layer from dry oil onto an inorganic surface of mica or glass. Dudasova et al.[28] concluded that asphaltene adsorption is due to polar interaction between surface and asphaltenes. Recently, our group has found that there is a correlation between asphaltene adsorption and aromaticities (lower H/C ratio) and nitrogen content in asphaltenes.[37] This work, in the absence of water, supports the conclusion made by our group that attributed adsorption to polar interactions between a solid surface and asphaltenes. These polar interactions are basically acid−base reactions occurring between adsorbate and adsorbant. From the results obtained so far, we conclude that basic oxides, for example, CaO and MgO, and amphoteric oxides, for example, Fe_3O_4 and Co_3O_4, demonstrate higher adsorption capacity as compared with acidic oxides, for example, TiO_2 and NiO. However, the quality of adsorption measured by adsorption affinity values (K_L) is higher for acidic oxides (with CaO being an exception). This suggests that strong interactions present between adsorbate and adsorbent may increase the catalytic effect of solids with high K_L values for various

dx.doi.org/10.1021/ef101230g |*Energy Fuels* 2011, 25, 1017–1023

Table 2. Estimated Parameters for the Langmuir and Freundlich Models at 25 °C

	Langmuir constants			Freundlich constants		
nanoparticles	Q_m (mg/m^2)	K_L (L/mg)	R^2	K_F (mg/m^2)(L/mg)$^{1/n}$	$1/n$ (unitless)	R^2
Co_3O_4	1.76	0.008	0.999	0.150	0.321	0.56
NiO	0.58	0.016	0.999	0.174	0.158	0.86
MgO	1.35	0.004	0.98	0.052	0.425	0.91
CaO	2.7	0.008	0.96	0.321	0.284	0.89
TiO_2	0.54	0.009	0.999	0.153	0.161	0.93
Fe_3O_4	1.7	0.005	0.999	0.095	0.376	0.94

reactions. Investigation of the effectiveness of K_L and Q_m upon the catalytic effect of various nanoparticles is beyond the scope of this work and shall be addressed in future work.

3.4. Adsorption Kinetics. Because NiO is a well-known catalyst used for many reactions[38−42] and it also showed high adsorption affinity toward asphaltenes in our study, it became significant to perform a kinetic study on adsorption of asphaltenes over NiO nanoparticles. The initial asphaltene concentration was kept at 500 ppm. Figure 4a shows that the solution color changed after mixing with NiO nanoparticles and became colorless after 2 h of mixing. Figure 4b shows the change in the amount of asphaltene adsorbed as a function of contact time. Evidently, the adsorption was very fast, as equilibrium was achieved in less than 2 h. This can be attributed to the external adsorption. As was evident in the BET measurement, NiO nanoparticles have no porous structure. Thus, external adsorption dominated, and no intraparticle diffusion was observed to slow down the adsorption rate. Similar observations were reported in our previous study with the adsorption of asphaltenes onto alumina nanoparticles.[43] It is worth noting that the equilibrium time for the adsorption of asphaltenes onto other reported adsorbents is much longer. For instance, long equilibration times for adsorption of asphaltenes on mineral surfaces have been reported by other researchers.[24,31,32,37,44−47]

3.5. Effect of Type of Asphaltene. Asphaltenes are precipitated using one of two main precipitants, namely, *n*-pentane[21,30,31,48,49] and *n*-heptane.[24,49−52] Each precipitant is reported to yield a precipitated asphaltene with different characteristics, that is, chemical composition, molar mass, and physical characteristics,[21,25] and different yields.[53] Therefore, the adsorption behavior will be different based on the type of precipitant. In this set of experiments, two different types of asphaltenes were tested for adsorption onto NiO nanoparticles at 25 °C. Two asphaltene samples were independently extracted from vacuum residue by adding *n*-pentane (C5) and *n*-heptane (C7), as explained in the Experimental Section. C7-asphaltenes and C5-asphaltenes were redissolved independently in toluene with the aim of obtaining an understanding on the effect of the type of asphaltene on the adsorption onto NiO nanoparticles. The results are shown in Figure 5. Both of the adsorption isotherms fit well to the Langmuir model. The maximum adsorption capacities and equilibrium constants are presented in Table 3. The maximum adsorption capacity of C5-asphaltenes is slightly lower than that of C7-asphaltenes. This can be attributed to the differences in the adsorption behavior of the selected asphaltenes. It should be noted that the presence of heteroatoms in asphaltenes makes them polar, so as a consequence, stronger interactions are expected. Also, because of high aromaticity in asphaltenes, bonding of π electrons to the empty d orbitals in transition-metal oxides cannot be over looked. It is known that

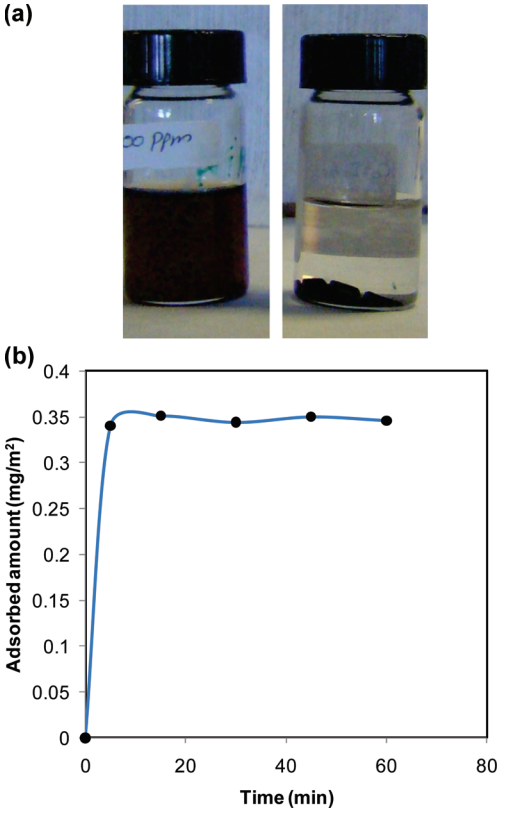

Figure 4. (a) Photos of a sample that was kept mixing for 2 h. Initial concentration of asphaltenes, 500 ppm; nanoparticle dose, 10 g/L; agitation speed, 200 rpm; *T*, 25 °C. (b) The adsorbed amount of asphaltenes onto NiO nanoparticles with the change of contact time at 500 ppm of initial concentrations of asphaltenes. Nanoparticle dose, 10 g/L; agitation speed, 200 rpm; *T*, 25 °C.

C7-asphaltenes are more polar and aromatic than C5-asphaltenes.[54] Also, the colloidal behavior and molecular mass and structure of the asphaltenes can play a role in adsorption as well. For instance, C5-asphaltenes contain higher amounts of resins than C7, and this would impact the colloidal behavior, which, in turn, affects the interactive forces between the asphaltenes molecules and NiO nanoparticles.[49] Nonetheless, the initial uptake by NiO nanoparticles appears similar for both types of asphaltenes.

3.6. Oxidation of Adsorbed Asphaltenes. Thermal analysis was performed in order to get more insight about the catalytic effect of nanoparticles on asphaltene oxidation. By performing simultaneous thermal analysis, both mass and heat changes with time can be monitored. The mass of the sample was kept to a minimum to avoid mass transfer (diffusion) limitations. Figures 6a,b show the profiles for the differential of mass loss

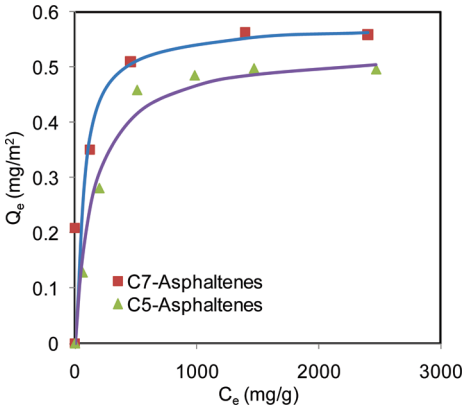

Figure 5. Adsorption isotherms of different types of asphaltenes onto NiO nanoparticles. Nanoparticle dose, 10 g/L; agitation speed, 200 rpm; *T*, 25 °C. Points are experimental data, and solid lines are from the Langmuir model (eq 1).

Table 3. Adsorption Capacities and Langmuir Constants of C7and C5 Asphaltenes at 25 °C

type	Q_m (mg/m²)	K_L (L/mg)	R^2
C7-asphaltenes	0.58	0.016	1
C5-asphaltenes	0.53	0.007	0.99

and heat changes, respectively, with the increase in temperature under an air atmosphere for C7-asphaltenes alone, as well as when adsorbed onto NiO nanoparticles. For pure C7-asphaltene oxidation, the mass loss profiles can be divided into two regions: (1) a low-temperature range up to 400 °C and (2) a high-temperature range beyond 400 °C. Because asphaltenes are heavy fractions of oil, no significant mass change can be observed before 400 °C. The mass loss profile shows that mass loss of pure asphaltene occurs in two steps, first, between 400 and 450 °C, showing low-temperature oxidation, the second beyond 450 °C, depicting complete oxidation to gaseous products. Because there is no exotherm associated with mass loss up to 450 °C in the heat changes profile (Figure 6b), we term this loss as the low-temperature oxidation region where the major mass loss occurs because of bond scission. Combustion in the presence of air occurs after 450 °C, as evidenced by the presence of an exotherm that follows the same profile as the mass loss. For the nanoparticles containing C7-asphaltenes, the profile of mass loss as well as heat evolved changed drastically. In the presence of NiO nanoparticles, combustion/oxidation of asphaltenes appears to happen at a much lower temperature (<325 °C). Actually, it appears that, when asphaltenes are adsorbed over NiO nanoparticles, the active sites over NiO catalyze the oxidation reaction, thus significantly lowering the temperature to around 150 °C, at which conversion commences. This decrease in combustion/oxidation temperature validates the idea that NiO nanoparticles catalyze the oxidation of asphaltenes considerably.

Activation energy can be calculated by processing simultaneous thermal analysis data. The Coats−Redfern method[55] is an integral method of processing the data that deals with only one weight loss curve to get the activation energy. The description of the method is as follows:

% conversion ratio (α) can be defined as

$$\alpha = \frac{w_0 - w_t}{w_0 - w_\infty} \tag{5}$$

where w_0 is the initial sample mass, w_∞ is the final sample mass, and w_t is the sample mass at any time.

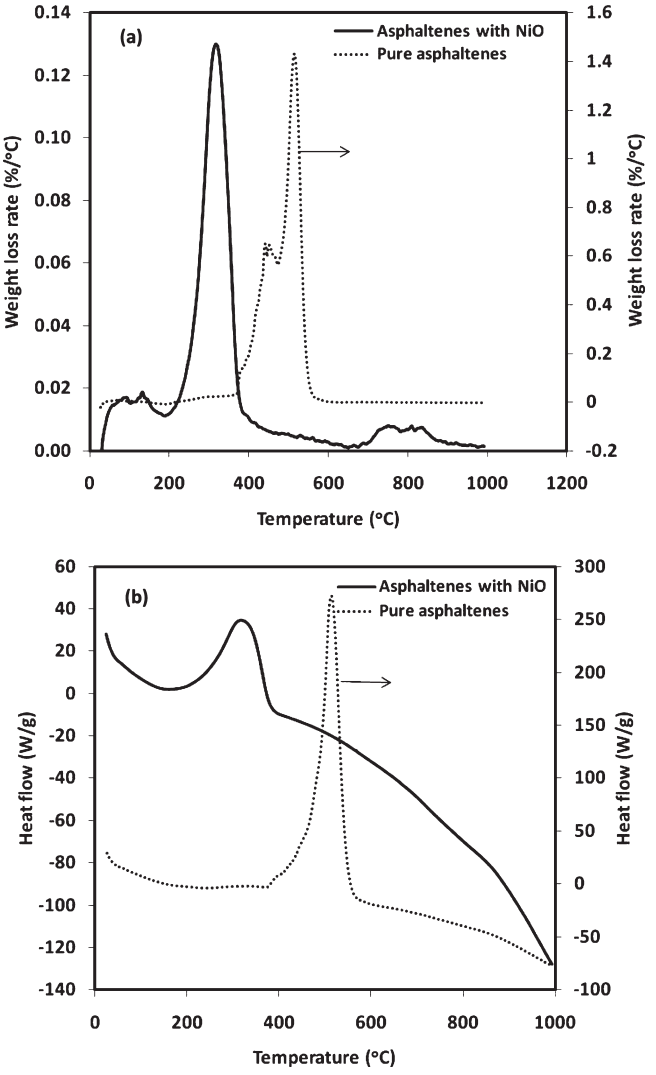

Figure 6. DTG−DTA curves for asphaltenes with and without NiO nanoparticles. (a) Plot of rate of mass loss as a function of temperature. (b) Plot of enthalpy changes as a function of temperature. Heating rate, 10 °C/min; air flow, 100 cm³/min.

The Arrehnius equation can be written in the following form to express the conversion rate

$$\frac{d\alpha}{dt} = Ae^{-E_a/RT} f(\alpha) \tag{6}$$

where $f(\alpha)$ is the mechanism function

If $f(\alpha) = (1 - \alpha)^n$, where n is the order of the reaction, then integration of eq 6 would yield

$$\int_0^\alpha \frac{d\alpha}{(1-\alpha)^n} = \frac{A}{\beta}\int_{T_0}^{T} \exp(-E_a/RT)dT \tag{7}$$

Equation 7 can be simplified to give eqs 8 and 9, for $n = 1$ and $n > 1$, respectively

$$-\frac{\ln(1-\alpha)}{T^2} = \frac{AR}{\beta E_a}\left(1 - \frac{2RT}{E_a}\right)\exp(-E_a/RT) \tag{8}$$

$$\frac{1-(1-\alpha)^n}{(1-\alpha)T^2} = \frac{AR}{\beta E_a}\left(1 - \frac{2RT}{E_a}\right)\exp(-E_a/RT) \tag{9}$$

dx.doi.org/10.1021/ef101230g |*Energy Fuels* 2011, 25, 1017–1023

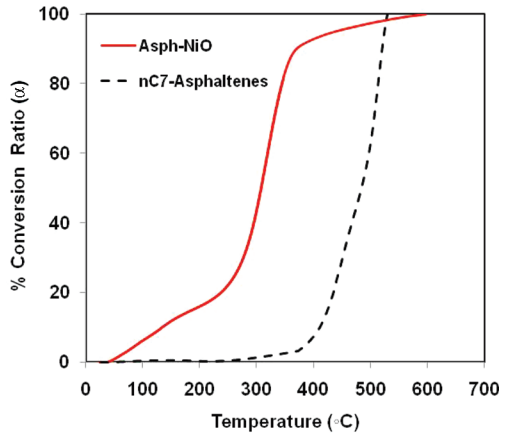

Figure 7. Asphaltene oxidation in the presence and absence of NiO nanoparticles.

Assuming that $[(2RT)/(E_a)] \ll 1.0$ and taking the natural (Napierian) logarithm on both sides, eqs 8 and 9 can also be written in linear form as follows

for $n = 1.0$

$$\ln \frac{-\ln(1-\alpha)}{T^2} = \ln\left(\frac{AR}{\beta E_a}\right) - \frac{E_a}{R} \times \frac{1}{T} \qquad (10)$$

for $n > 1.0$

$$\ln \frac{1-(1-\alpha)^n}{(1-\alpha)T^2} = \ln\left(\frac{AR}{\beta E_a}\right) - \frac{E_a}{R} \times \frac{1}{T} \qquad (11)$$

If n is known, then a plot of the left-hand-side of eq 10 or 11 versus $1/T$ would give a straight line with a slope = E_a/R.

Figure 7 shows a plot of the percent conversion ratio or the extent of the reaction, α, of asphaltenes with and without nanoparticles as a function of temperature, where α was estimated as per eq 5. In the absence of nanoparticles, mass loss (in considerable amounts) occurred beyond 350 °C and reached a maximum rate at around 475 °C, showing occurrence of a combustion reaction during oxidation. It is evident from the figure that the presence of NiO nanoparticles greatly enhances the oxidation process. The oxidation process involving thermal cracking starts as early as 150 °C. The rate of oxidation reaches its maximum around 300 °C. This lowering of temperature shows the catalytic behavior of NiO on oxidation of asphaltenes. Activation energies for the overall reaction were calculated using the Coats−Redfern method. Figure 8 shows a plot of $\ln\{[-\ln(1-\alpha)]/T^2\}$ versus $1/T$ that should ideally give a straight line with slope = E_a/R, where E_a is the activation energy (kJ/mol) and R is the ideal gas constant (8.314 J/mol·K). However, in our case, deviation from the straight line showed the presence of competitive reactions or a change in the reaction mechanism. Other researchers have also observed similar behavior, that is, a curved/bent line, and have used this method to calculate the activation energies.[56,57] The presence of NiO nanoparticles causes a drop of activation energy by approximately 100 kJ/mol, showing its catalytic effect. Oxidation of asphaltenes in the absence of nanoparticles showed three distinct regions, as seen in Figure 8: low-temperature (372−467 °C), mid-temperature (467−514 °C), and high-temperature (over 514 °C) oxidation, depicting oxidation of different types of carbons present in the system. However, in the presence of nanoparticles, the oxidation temperature decreased by ∼100 °C, showing their catalytic effect.

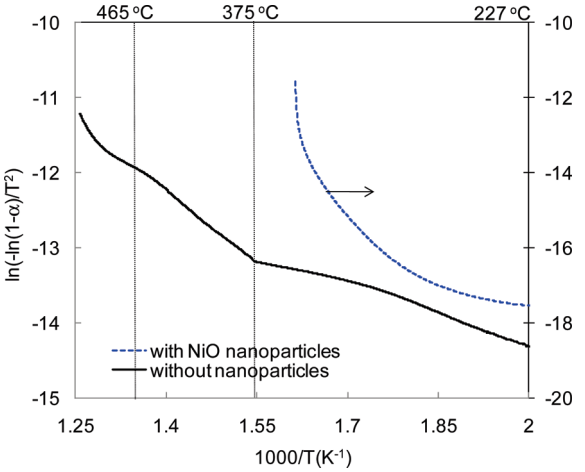

Figure 8. Oxidation of asphaltenes with and without NiO nanoparticles.

4. CONCLUSIONS

Our study on nanoparticles showed that nanoparticles can adsorb asphaltenes from model heavy oil efficiently. The Langmuir adsorption isotherm model gives a good fitting for the adsorption isotherms, suggesting a monolayer adsorption. CaO showed the highest adsorption capacity (Q_m) but not the highest adsorption affinity (K_L) at the same temperature and equilibrium concentration. This shows that the extent of adsorption and the quality of adsorption are not always related. Oxidation of asphaltenes in the absence of nanoparticles showed three distinct regions, depicting oxidation of different types of carbons present in the system. The presence of NiO nanoparticles with asphaltenes caused a significant decrease in the oxidation temperature and activation energy showing their catalytic effect.

This study supports that nanoparticles could be applied for heavy oil upgrading and processing with a cost-effective approach, as they could be prepared *in situ*. Our study has the potential to be developed into a future technology that may have a huge effect on the industrial and environmental impact.

■ AUTHOR INFORMATION

Corresponding Author

*E-mail: ppereira@ucalgary.ca.

■ ACKNOWLEDGMENT

The authors acknowledge the financial support provided by Carbon Management Canada Inc. (CMC).

■ REFERENCES

(1) Nassar, N. N.; Husein, M. M. In *The IASTED International Conference on Environmental Management and Engineering (EME 2009)*, Banff, Canada, July 6−8, 2009; ACTA Press: Calgary, Alberta, Canada, 2009; pp 135−138.

(2) Nassar, N. N.; Husein, M. M. *Fuel Process. Technol.* **2010**, *91*, 164–168.

(3) Nassar, N. N.; Husein, M. M.; Pereira-Almao, P. *Fuel Process. Technol.* **2010**, *91*, 169–174.

(4) *Environmental Management of Alberta's Oil Sands*; Governement of Alberta, http://environment.gov.ab.ca/info/library/8042.pdf, (accessed August 1, 2010).
(5) Husein, M. M.; Nassar, N. N. *Curr. Nanosci.* **2008**, *4*, 370–380.
(6) Husein, M. M.; Patruyo, L.; Pereira-Almao, P.; Nassar, N. N. *J. Colloid Interface Sci.* **2010**, *342*, 253–260.
(7) Tratnyek, P. G.; Johnson, R. L. *Nano Today* **2006**, *1*, 44–48.
(8) Nassar, N. N. *Sep. Sci. Technol.* **2010**, *45*, 1092–1103.
(9) Nassar, N. N. *J. Hazard. Mater.* **2010**, *184*, 538–546.
(10) Mousavi-Dehghani, S. A.; Riazi, M. R.; Vafaie-Sefti, M.; Mansoori, G. A. *J. Pet. Sci. Eng.* **2004**, *42*, 145–156.
(11) Bockrath, B. C.; LaCount, R. B.; Noceti, R. P. *Fuel* **1980**, *59*, 621–626.
(12) Rosales, S.; Machiín, I.; Sánchez, M.; Rivas, G.; Ruette, F. *J. Mol. Catal. A: Chem.* **2006**, *246*, 146–153.
(13) Sheu, E. Y.; Shields, M. B.; Storm, D. A. *Fuel* **1994**, *73*, 1766–1771.
(14) Wargadalam, V. J.; Norinaga, K.; Iino, M. *Fuel* **2002**, *81*, 1403–1407.
(15) Wallace, P. S.; Anderson, M. K.; Rodarte, A. I.; Preston, W. E. In *Gasification Technologies Conference*, San Francisco, CA, 1998.
(16) Benbouzid, M.; Hafsi, S. *Fuel* **2008**, *87*, 1585–1590.
(17) Indrijarso, S.; Oklany, J. S.; Millington, A.; Price, D.; Hughes, R. *Thermochim. Acta* **1996**, *277*, 41–52.
(18) Kök, M. *J. Therm. Anal. Calorim.* **2002**, *68*, 1061–1077.
(19) Teman, M.; Kriz, J. F. *Pet. Sci. Technol.* **1998**, *16*, 167–178.
(20) Kumar, K.; Dao, E.; Mohanty, K. K. *J. Colloid Interface Sci.* **2005**, *289*, 206–217.
(21) Marlow, B. J.; Sresty, G. C.; Hughes, R. D.; Mahajan, O. P. *Colloids Surf.* **1987**, *24*, 283–297.
(22) Freundlich, H. M. F. Z. *Phys. Chem.* **1906**, *57(A)*, 385–470.
(23) Langmuir, I. *J. Am. Chem. Soc.* **1916**, *38*, 2221–2295.
(24) Toulhoat, H.; Prayer, C.; Rouquet, G. *Colloids Surf., A* **1994**, *91*, 267–283.
(25) Evdokimov, I. N.; Eliseev, N. Y.; Akhmetov, B. R. *J. Pet. Sci. Eng.* **2003**, *37*, 135–143.
(26) Angle, C. W.; Long, Y.; Hamza, H.; Lue, L. *Fuel* **2006**, *85*, 492–506.
(27) Marczewski, A. W.; Szymula, M. *Colloids Surf., A* **2002**, *208*, 259–266.
(28) Dudásová, D.; Simon, S.; Hemmingsen, P. V.; Sjöblom, J. *Colloids Surf., A* **2008**, *317*, 1–9.
(29) Rana, M. S.; Sámano, V.; Ancheyta, J.; Diaz, J. A. I. *Fuel* **2007**, *86*, 1216–1231.
(30) Alkafeef, S. F.; Algharaib, M. K.; Alajmi, A. F. *J. Colloid Interface Sci.* **2006**, *298*, 13–19.
(31) Dean, K. R.; McAtee, J. L., Jr. *Appl. Clay Sci.* **1986**, *1*, 313–319.
(32) González, M. F.; Stull, C. S.; López-Linares, F.; Pereira-Almao, P. *Energy Fuels* **2006**, *21*, 234–241.
(33) Groenzin, H.; Mullins, O. C. *Energy Fuels* **2000**, *14*, 677–684.
(34) Fritschy, G.; Papirer, E. *Fuel* **1978**, *57*, 701–704.
(35) El-Sabagh, S. M. *Fuel Process. Technol.* **1998**, *57*, 65–78.
(36) Drummond, C.; Israelachvili, J. *J. Pet. Sci. Eng.* **2004**, *45*, 61–81.
(37) López-Linares, F.; Carbognani, L.; Sosa-Stull, C.; Pereira-Almao, P.; Spencer, R. J. *Energy Fuels* **2009**, *23*, 1901–1908.
(38) El Shobaky, G.; Gravelle, P. C.; Teichner, S. J. In *Oxidation of Organic Compounds*; The American Chemical Society: Washington, DC, 1968; pp 292−312.
(39) Elliott, D. C. *Energy Fuels* **2007**, *21*, 1792–1815.
(40) Li, J.; Yan, R.; Xiao, B.; Liang, D. T.; Du, L. *Environ. Sci. Technol.* **2008**, *42*, 6224–6229.
(41) Ruckenstein, E.; Hu, Y. H. *Ind. Eng. Chem. Res.* **1998**, *37*, 1744–1747.
(42) Vann, W. D.; Castleman, A. W. *J. Phys. Chem. A* **1999**, *103*, 847–857.
(43) Nassar, N. N. *Energy Fuels* **2010**, *24*, 4116–4122.
(44) Kokal, S.; Tang, T.; Schramm, L.; Sayegh, S. *Colloids Surf., A* **1995**, *94*, 253–265.
(45) Gaboriau, H.; Saada, A. *Chemosphere* **2001**, *44*, 1633–1639.
(46) Carbognani, L.; González, M. F.; Lopez-Linares, F.; Sosa Stull, C.; Pereira-Almao, P. *Energy Fuels* **2008**, *22*, 1739–1746.
(47) López-Linares, F.; Carbognani, L.; Stull, C. S.; Pereira-Almao, P. *Energy Fuels* **2008**, *22*, 2188–2194.
(48) Szymula, M.; Marczewski, A. W. *Appl. Surf. Sci.* **2002**, *196*, 301–311.
(49) Ekholm, P.; Blomberg, E.; Claesson, P.; Auflem, I. H.; Sjöblom, J.; Kornfeldt, A. *J. Colloid Interface Sci.* **2002**, *247*, 342–350.
(50) Abdallah, W. A.; Taylor, S. D. *Nucl. Instrum. Methods Phys. Res., Sect. B* **2007**, *258*, 213–217.
(51) Sztukowski, D. M.; Jafari, M.; Alboudwarej, H.; Yarranton, H. W. *J. Colloid Interface Sci.* **2003**, *265*, 179–186.
(52) González, G.; Middea, A. *Colloids Surf.* **1991**, *52*, 207–217.
(53) Strausz, O. P.; Peng, P.; Murgich, J. *Energy Fuels* **2002**, *16*, 809–822.
(54) Long, R. B. In *Chemistry of Asphaltenes*; The American Chemical Society: Washington, DC, 1982; Vol. 195, pp 17−27.
(55) Coats, A. W.; Redfern, J. P. *Nature* **1964**, *201*, 68–69.
(56) Yanagisawa, K.; Suzuki, T. *Fuel* **1993**, *72*, 25–30.
(57) He, B. L.; Song, Q.; Xu, S.; Yao, Q. In *5th Asia-Pacific Conference on Combustion*; The University of Adelaide: Adelaide, Australia, 2005; pp 253−256.